Journal of Alloys and Compounds, 187 (1992) 113–135
JALCOM 295

Investigation of hydriding properties of $LaNi_{4.8}Sn_{0.2}$, $LaNi_{4.27}Sn_{0.24}$ and $La_{0.9}Gd_{0.1}Ni_5$ after thermal cycling and aging

Steven W. Lambert, Dhanesh Chandra and William N. Cathey
University of Nevada, Reno, NV 89557 (USA)

Franklin E. Lynch
Hydrogen Consultants Inc., 12400 North Dumont Way, Littleton, CO 80125 (USA)

Robert C. Bowman Jr.
Aerojet Electronic Systems Division, P.O. Box 296, Azusa, CA 91702 (USA)

(Received December 16, 1991; in final form March 2, 1992)

Abstract

Thermal degradation studies were conducted on hydrides formed by Sn and Gd substituted $LaNi_5$ compounds. Static room temperature pressure–composition isotherms were measured after 10, 1500 and 10 000 cycles and after thermal aging to evaluate changes in the properties. The hydrogen absorption properties of $La_{0.9}Gd_{0.1}Ni_5$ seriously degraded in both prolonged thermal cycling and aging tests but the $LaNi_{4.8}Sn_{0.2}$ and $LaNi_{4.27}Sn_{0.24}$ hydrides were virtually unaffected. In the case of $La_{0.9}Gd_{0.1}Ni_5$ the lattice microstrains were significantly larger and the domain sizes smaller as compared with those of $LaNi_{4.8}Sn_{0.2}$ after thermal cycling, but the majority of the strains were accumulated during the first 10 activation cycles. After 10 000 cycles the hydride of $la_{0.9}Gd_{0.1}Ni_5$ becomes either amorphous or microcrystalline, whereas the hydride of $LaNi_{4.8}Sn_{0.2}$ is well crystallized.

1. Introduction

Rare earth intermetallic compounds, such as $LaNi_5$, of hexagonal structure ($CaCu_5$ type) are of interest as thermal storage media. One of the applications of interest in the present study is in metal hydride heat pumps (MHHP) for space suits in the extravehicular mobility units (EMUs) [1]. The EMU has two heat exchangers, each containing metal hydrides with slightly different chemical affinities for hydrogen, *i.e.* different plateau pressures. Substituted $LaNi_{4.8}Sn_{0.2}$ was used for the low pressure hydride [2] and $La_{0.9}Gd_{0.1}Ni_5$ for the high pressure hydride [3]. Degradation of the properties of hydrides, such as the loss of absorption/desorption capacity of hydrogen, is detrimental for an EMU metal hydride heat pump in long-term use. Several studies have been conducted to establish the effect of long-term thermal cycling on the hydrogen capacity of $LaNi_5$ and its substituted alloys [4–11]. These studies have shown that the degradation is dependent on the substituting element in $LaNi_5$ hydrides. A possible reason for degradation is extrinsic interaction

0925-8388/92/$5.00

with gaseous impurities during thermal cycling. For example, Gamo *et al.* [4] reported 60% loss in capacity of $LaNi_5$ after 3700 cycles by introducing hydrogen gas during every cycle. If the cycling is performed in a closed loop apparatus and fresh hydrogen is not introduced at every cycle then extrinsic contamination should be reduced. Intrinsic degradation of hydrides is likely to occur when these materials are subjected to thermal cycles. Pioneering studies by Cohen *et al.* [5, 6] reported disproportionation of $LaNi_5$ to LaH_2 and microphase nickel after thermal cycling. Cohen *et al.* [6] used Mössbauer methods and thermal desorption experiments to infer the presence of LaH_2 and Ni, but these phases were not confirmed by X-ray diffraction methods, possibly due to the microcrystalline or amorphous nature of the products. Benham and Ross [7] did not detect the presence of LaH_2 phase by inelastic neutron diffraction methods after subjecting $LaNi_5$ to 750 thermal cycles. Buschow and Meidema [8] suggested that disproportionation may be due to the metastable nature of the hydrides. There is always a loss of hydrogen capacity [6, 9] when thermal degradation of $LaNi_5$ occurs. Thermal cycling studies on $LaNi_5$ by Park and Lee [9] showed a loss of 62% in hydrogen uptake capacity after 3500 cycles.

Josephy *et al.* [10] observed some degradation of $LaNi_5$ after 45 000 thermal cycles and described the changed structural properties. Mordkovich *et al.* [11] investigated the degradation of $LaNi_5$ after up to 7000 cycles and reported formation of an intermediate phase, $LaNi_5H_4$, during thermobaric cycling. Matsumoto *et al.* [12] and Nomura *et al.* [13] and others have also reported observing $LaNi_5H_4$. Abika *et al.* [14] confirmed the existence of the intermediate $LaNi_5H_x$ phase but reported its stoichiometry as $LaNi_5H_3$.

The degradation behavior of substituted compounds of $LaNi_5$ is dependent on the type of substitutional element added. Park and Lee [9] have reported good resistance to degradation during thermal cycling of $LaNi_{4.7}Al_{0.3}$ with a loss of 12% in hydrogen uptake capacity after 2500 cycles. They have suggested [9] that electronic and geometric effects are responsible for the increased stability of this compound due to the introduction of Al in a 3g position in the lattice of $LaNi_5$. Goodel [15] found essentially no intrinsic degradation of $LaNi_{4.7}Al_{0.3}$ after 1500 pressure cycles at 85 °C. He suggested that the larger Al atom interfered with the diffusion of the La atom from its original 1a site to the neighboring 2c or 3g sites, stabilizing the Ni sublattice by strong interactions with nickel (Ni_3Al). Kim and Lee [16] investigated the degradation of $MmNi_{4.5}Al_{0.5}$ and $MmNi_{4.15}Fe_{0.85}$ and found good resistance to cycling with a loss of 7.6% and 6% in uptake capacity respectively after 3000 cycles.

In the present paper we report differences in the intrinsic degradation behavior of high and low pressure $La_{0.9}Gd_{0.1}Ni_5$ and $LaNi_{4.8}Sn_{0.2}$ hydrides respectively. These experiments were performed by thermal absorption and desorption of hydrogen for up to 10 000 cycles by observing the changes in static pressure–composition isotherms of compounds after thermal cycling. Polycrystalline X-ray diffraction analyses were performed to determine the crystal structure and to measure microstrain distribution/particle size effects

in dehydrided cycled materials. In addition, thermal aging experiments were also performed to observe the degradation of these Gd and Sn substituted $LaNi_5$ compounds and the results were compared with those of the thermally cycled materials. These thermal aging experiments were performed based on the method of Sandrock *et al.* [17].

2. Experimental procedures

2.1. Materials and alloy preparation

Lanthanum (99%), nickel (99.9%), gadolinium (99 + %), indium (99.99%) and tin (99.997%) were used in this study. The $La_{0.9}Gd_{0.1}Ni_5$ alloy was arc-melted in an argon atmosphere and used in the as-cast condition. A few experiments performed on the annealed and as-cast materials did not reveal any significant changes in the pressure–composition isotherms. The $LaNi_5$ with Sn additive was prepared by arc-melting and heat treated at 950 °C for 90 h. The stoichiometry was strictly $LaNi_{4.8}Sn_{0.22}$ but is nominally referred to as $LaNi_{4.8}Sn_{0.2}$. The thermal aging experiments were performed at 180 °C on $La_{0.9}Gd_{0.1}Ni_5$ and $LaNi_{4.27}Sn_{0.24}$. The formula for $LaNi_{4.27}Sn_{0.24}$ may be expressed as $La_{1.11}Ni_{4.37}Sn_{0.27}$ with excess La atoms, to show that Ni/Sn ratio of $LaNi_{4.8}Sn_{0.22}$ and $La_{1.11}Ni_{4.73}Sn_{0.27}$ are similar.

2.2. Hydriding, cycling and thermal aging experiments

A conventional Sievert's apparatus was used to obtain static pressure–composition isotherms before and after thermal cycling or thermal aging. Isotherms were also taken over a range of temperature to establish the van't Hoff relationship. The cyclic test apparatus, in which the reactors were heated to 125 °C and cooled to room temperature by forced air cooling is shown schematically in Fig. 1(a). The pressure changes during thermal cycling reflected saturated conditions at lower temperatures and depleted conditions at higher temperatures.

Twelve grams of intermetallics were loaded in separate standard hydride reactors for cyclic thermal degradation studies. The samples were first activated on the Sievert's apparatus and isotherms were measured at 25 °C to establish baseline characteristics. The reactors were then attached to small pressure vessels, each equipped with a pressure gauge, as shown in Fig. 1(a). Prior to opening the reactor valve, the pressure vessels were heated to 125 °C and then cooled to room temperature while flushing several times with high purity hydrogen (99.999%). To assure complete conversion of α- to β-phase the reactors were cooled to room temperature during each thermal cycle.

The sample holder with high pressure $La_{0.9}Gd_{0.1}Ni_5$ hydride was attached to a 75 cm^3 pressure vessel and the low pressure $LaNi_{4.8}Sn_{0.2}$ hydride to a 500 cm^3 vessel. The 500 cm^3 pressure vessel had enough volume to receive the hydrogen discharged at 125 °C. The pressure gauges and thermocouples provided a simple way of checking on the performance. The thermal cycling was performed for several months, charging and discharging once every

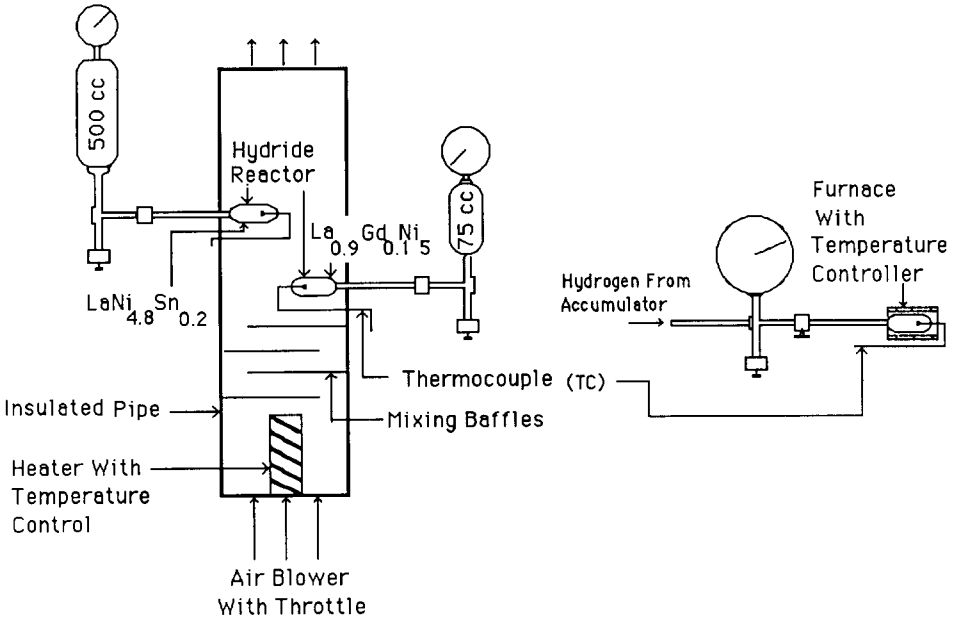

Fig. 1. (A) Heating cooling apparatus for long-term thermal cycling; (B) high pressure thermal aging apparatus.

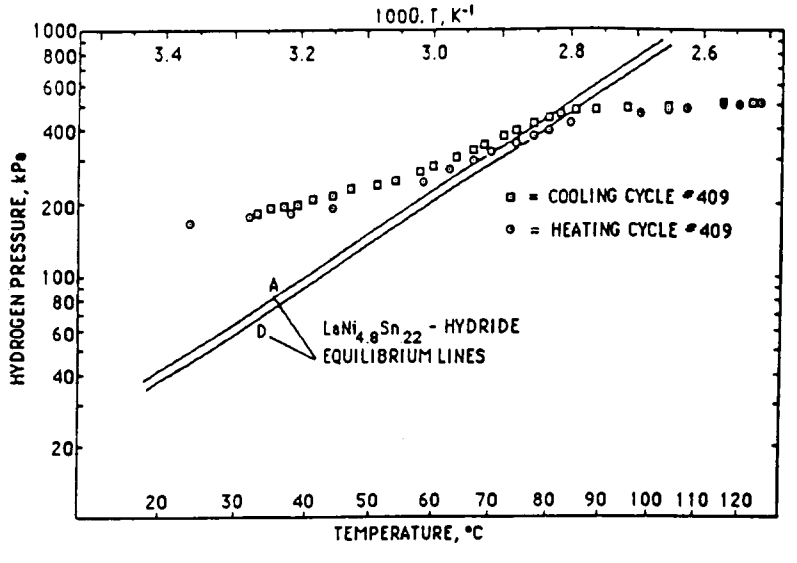

Fig. 2. A typical cycling of hydride is shown for $LaNi_{4.8}Sn_{0.22}$. By heating from room temperature to 125 °C one can start from saturated condition to depleted condition (below the equilibrium line).

hour. A typical curve during a heating cycle for the $LaNi_{4.8}Sn_{0.2}$ is shown in Fig. 2. The pressures observed in the reactor at 24, 60 and 85 °C were 170, 250 and 450 kPa respectively. Heating above 85 °C to 125 °C raised the pressure from 450 kPa to 510 kPa and the reversible hydrogen in the system was fully discharged. The major change in pressure occurred during the $\beta \rightarrow \alpha$ transition in the range of pressures and temperatures corresponding to the van't Hoff equilibrium lines, also shown in Fig. 2.

The maximum cycle pressures indicated a loss in capacity of a few per cent, probably due to defect trapping, as described by Lynch and Reilly [18] during the first hundred or so cycles. The sample holders from the cycling and aging apparatuses, shown in Fig. 1, were connected to a Sievert's apparatus to obtain isotherms. Appropriate precautions were taken to prevent contamination. Isotherms were obtained after 10, 1500 and 10 000 thermal cycles and after thermal aging.

The thermal aging experiments were performed using the same type of sample holder as the one used in the thermal cycling studies in an apparatus shown in Fig. 1(b). A metal hydride compressor with ultrapure hydrogen source was used to attain 20 700 kPa for these experiments and the pressure was measured by using a Heise gauge (0–20 700 kPa). The samples were heated by a small tubular heater. The experimental procedure for $La_{0.9}Gd_{0.1}Ni_5$ is described as follows. The samples were first subjected to 10 activation cycles, and on the 11th cycle a pressure–composition isotherm was taken

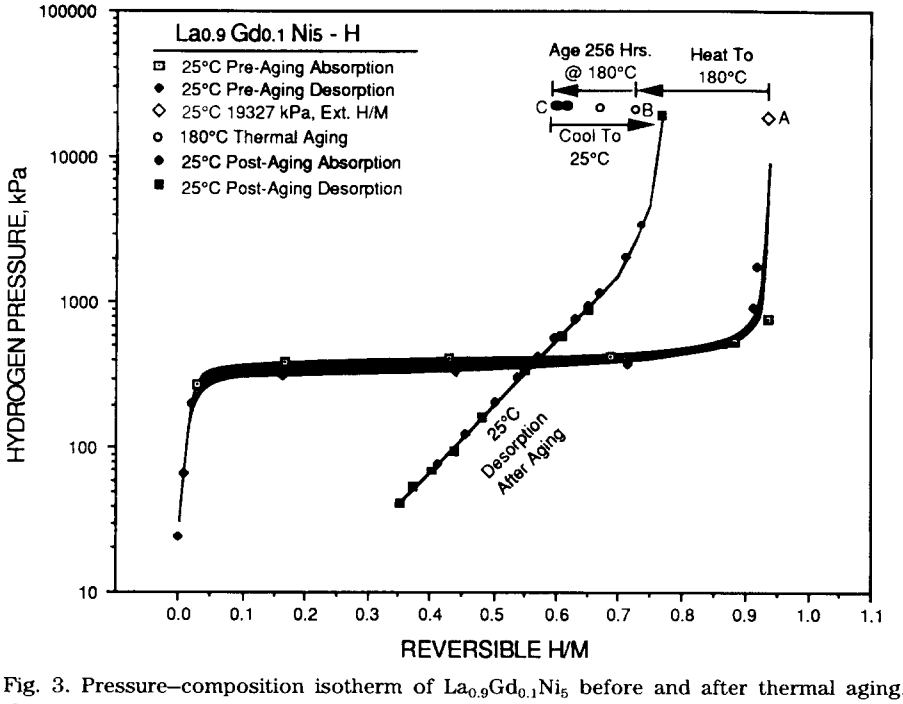

Fig. 3. Pressure–composition isotherm of $La_{0.9}Gd_{0.1}Ni_5$ before and after thermal aging. Also shown are the intermediate pressures and H/M ratios during thermal aging.

at 25 °C (see Fig. 3). The samples were then transferred to the thermal aging apparatus and heated to 180 °C and a pressure of 19 327 kPa was obtained with decreases in the H/M (hydrogen/metal) ratio, as indicated by the left arrow. The pressure continued to increase with time, associated with decreases in H/M. This thermal aging treatment was continued at 180 °C for 256 h, at which time the H/M ratio was about 0.76; (point C in Fig. 3). The sample was then cooled to 25 °C and the H/M ratio increased to roughly 0.76 (point B), but not to the original value of 1.1 (point A). Thus, a decrease in capacity of roughly 19.6% was observed after thermal aging at 19 MPa for 260 h at 435 K. After completion of the post-aging studies, the hydrogen was baked out and the pressures obtained during the baking were recorded.

A vacuum glove box was connected to an ultrahigh purity hydrogen supply at HCI. This glove box was evacuated to 10^{-3} Torr and back-filled with hydrogen three times. A refrigerated aluminum block was placed in the glove box to allow hydride specimen preparation. This preparation included grinding and filling the samples with hydrides into quartz capillaries at 255 K. A majority of the hydrides remain fully charged at this temperature with a hydrogen pressure of 83 kPa. The capillaries were sealed with epoxy with quick setting cement.

2.3. X-ray diffraction experiments

Crystal structure studies were conducted on these intermetallics before and after hydriding using X-ray powder diffraction (XRPD) analyses. The hydrided materials were mixed with an NBS-680 silicon standard and sealed in quartz capillaries in the hydrogen filled glove box, in order to maintain the hydrided conditions. A special sample holder was made to accommodate the hydrided materials in 0.5 or 1 mm diameter quartz capillaries. The capillaries were mounted on the diffractometer, with minimum displacement errors. An APD 3720 Philips X-ray diffraction system with a graphite monochromator was used to obtain most of the diffraction data. X-ray powder diffraction (XRPD) patterns of $La_{0.9}Gd_{0.1}Ni_5$ hydride were also obtained using a Rigaku system equipped with a rotating anode (Cu) X-ray tube with higher tube power than a conventional X-ray tube. The background counts for the hydrides were high, due to scattering from the capillaries.

2.4. Microstrain distribution and domain size calculations using line broadening analyses

Line broadening analyses were used to determine the microstrain and particles sizes. The crystallite size and microstrain can be determined with high accuracy if Warren–Averbach analyses are performed on two or more orders of a particular reflection. If the broadening is not substantial for the peaks in question and peak overlap occurs then this method is not suitable. There are several other approaches, for example, gaussian and Cauchy methods [19] which use a single or multiple line. In the case of $La_{0.9}Gd_{0.1}Ni_5$, where the line broadening was significant, Warren–Averbach analyses were performed and checked with a multiple-line Cauchy method [19]. The Cauchy method

was used for profile analyses of $LaNi_{4.8}Sn_{0.2}$ because of the relatively small broadening of the peaks. A high purity $LaNi_5$ annealed powder was used as standard to correct the instrumental broadening.

In the Warren–Averbach method, the Stokes-corrected broadened profiles were used to calculate cosine coefficients. The domain size and strain broadening are separated by using the following relationship [20]:

$$\ln[A(L)] = \ln[A^P(L)] - [(2\pi^2 L^2 \cdot \langle e^2 \rangle)/d] \quad (1)$$

where L is the distance perpendicular to the diffracting plane, $A(L)$ is the Fourier cosine coefficient, $A^P(L)$ is the size term, $\langle e^2 \rangle$ is the mean square of the strain over a distance L. The value of d (Å) for a particular (h, k, l) is obtained in terms of lattice parameters using the following equation:

$$(1/d^2) = 4/3[(h^2 + hk + k^2)/a^2] + (l^2/c^2) \quad (2)$$

The Cauchy multiple peak method was used for line profiles for $LaNi_{4.8}Sn_{0.2}$. In this method, if the broadening is due to both the strain and particle size effects the following equation may be applied:

$$\beta c(\cos\theta) = K\lambda/D + 4e \sin\theta \quad (3)$$

where $K \sim 1$. The maximum strain, e, is related to the r.m.s. strain by [19]:

$$\langle \epsilon^2 \rangle^{1/2} = e/1.25 \quad (4)$$

Plotting $\beta c(\cos\theta)$ *vs.* $4\sin\theta$, the slope gives the strain e and the intercept gives λ/D from which D can be calculated. Although the strain in a specific direction may be obtained by the multiple peak method, in this case average values are projected for the intermetallic. The calculated strains give the upper limit of the lattice distortions.

3. Results

3.1. The system $La_{0.9}Gd_{0.1}Ni_5$ hydrogen

The static pressure–composition isotherms for $La_{0.9}Gd_{0.1}Ni_5$ obtained before thermal cycling are presented in Fig. 4. Absorption/desorption plateau pressure ratios of 150/120, 3540/300, 2000/1650 (in KPa) are observed at 4, 25 and 75 °C respectively, with lowering of hydrogen capacity. The plateaus obtained are nearly horizontal showing complete conversion of α- to β-phase at 4 and 25 °C, but there is a possible splitting of the desorption plateau at the higher hydrogen concentration obtained at 75 °C. The temperature dependence of α- and β-phase regions as represented by pressures in the middle of the plateaus are shown in the van't Hoff plots in Fig. 5.

The room temperature pressure–composition isotherms of $La_{0.9}Gd_{0.1}Ni_5$ for 10, 1500 and 10 000 cycled samples are shown in Fig. 6. In these reversible H/M isotherms the initial H/M is made zero at the start of the cycle for comparison purposes. The hydrogen trapped in the crystal lattice is not quantifiable and is included in the net decrease in hydrogen capacity.

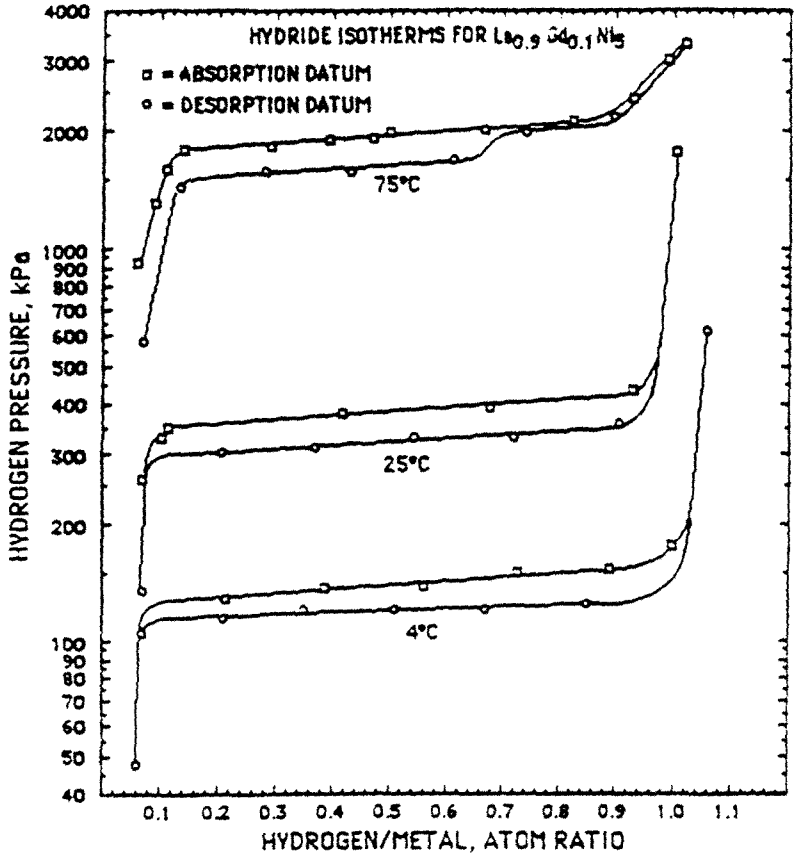

Fig. 4. Hydrogen pressure *vs.* hydrogen content in $La_{0.9}Gd_{0.1}Ni_5$ at 4, 25 and 75 °C.

The plateau develops a slope after 1500 cycles and this slope increases after 10 000 cycles. After 1500 and 10 000 cycles approximately 83% and 20% respectively, of the original hydrogen capacity remains. Figure 3 shows the loss of hydrogen capacity upon thermal aging of $La_{0.9}Gd_{0.1}Ni_5$ and Fig. 7 shows that the majority of the loss took place during the first 100 h. Post-aging absorption and desorption isotherms reveal a loss in the hydrogen capacity of 63% (at 430 kPa), also shown in Fig. 3.

The XRPD patterns of $La_{0.9}Gd_{0.1}Ni_5$, in as-prepared, after 10 and 10 000 hydriding cycles are shown in patterns A, B and C respectively, in Fig. 8. The Bragg peaks in pattern B are accounted for by the $CaCu_5$ type of hexagonal structure of the original alloy $La_{0.9}Gd_{0.1}Ni_5$ shown in pattern A. However, in the 10 000 cycled (desorbed) $La_{0.9}Gd_{0.1}Ni_5$, additional peaks whose *d*-spacings match that of f.c.c. nickel phase are observed in pattern C. The Bragg peaks of $La_{0.9}Gd_{0.1}Ni_5$ phase after 10 and 10 000 cycles are significantly broadened as compared with the alloy, indicating microstrain and/or small particle-size effects [19, 20].

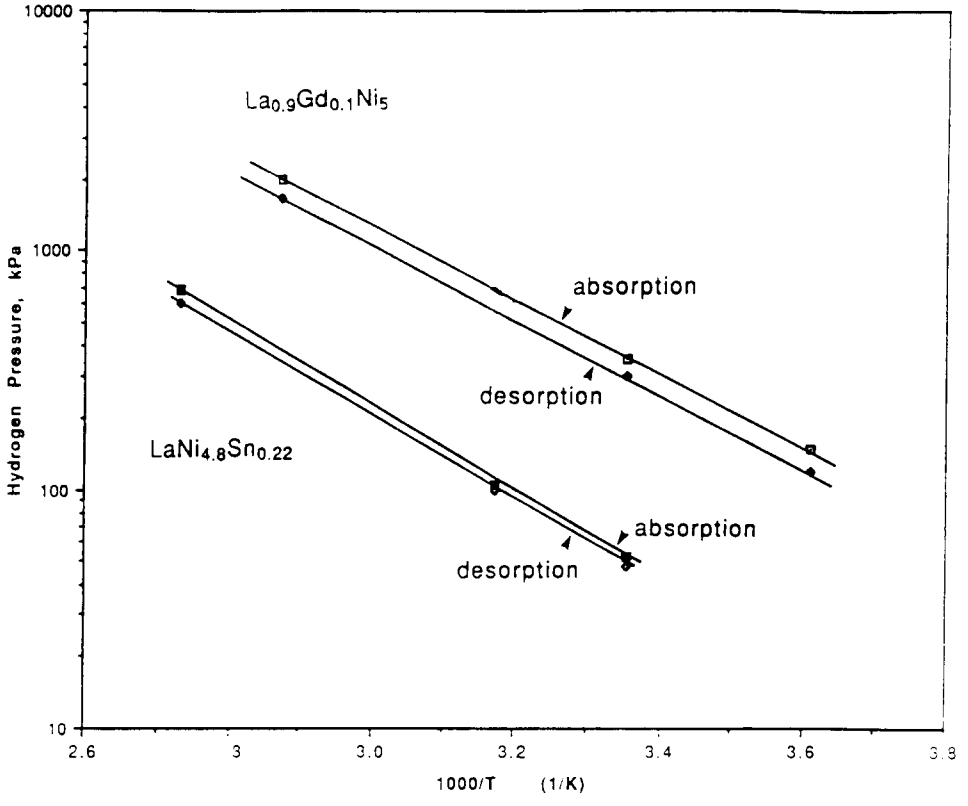

Fig. 5. van't Hoff plots for $La_{0.9}Gd_{0.1}Ni_5$ and $LaNi_{4.8}Sn_{0.22}$ (absorption and desorption).

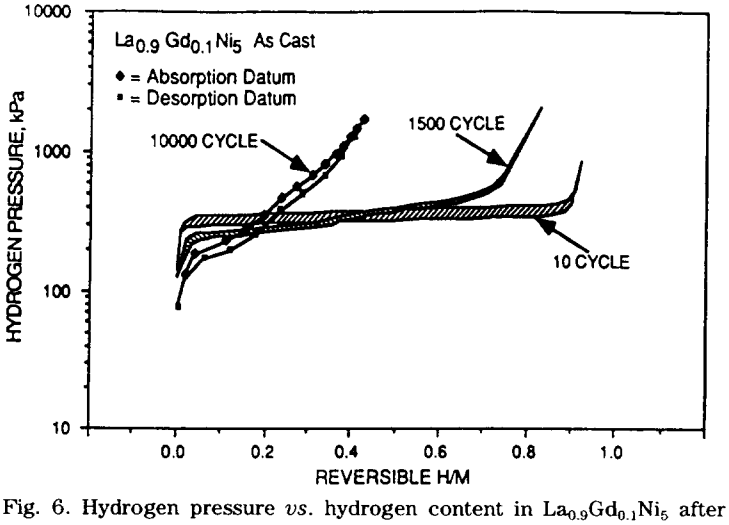

Fig. 6. Hydrogen pressure *vs.* hydrogen content in $La_{0.9}Gd_{0.1}Ni_5$ after 10, 1500 and 10 000 cycles, showing loss of hydrogen capacity after many cycles.

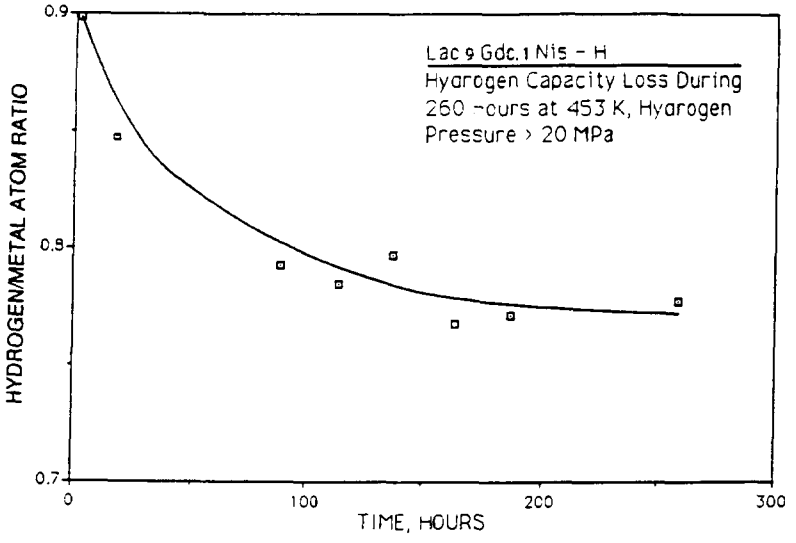

Fig. 7. Degradation of $La_{0.9}Gd_{0.1}Ni_5$ hydride during thermal aging was most rapid during the first 100 h.

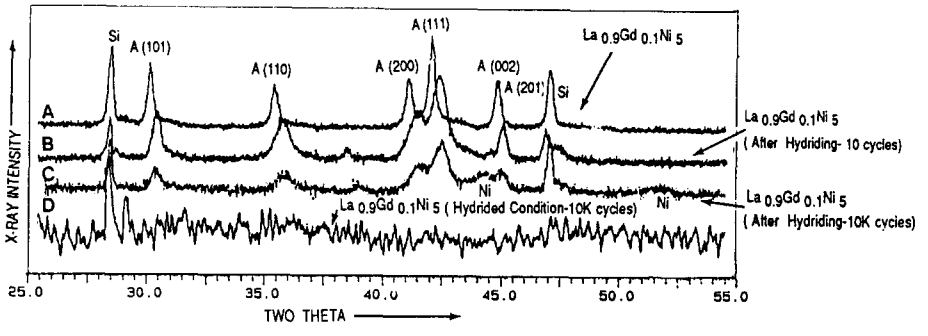

Fig. 8. X-ray diffraction patterns of $La_{0.9}Gd_{0.1}Ni_5$. Pattern (A) is obtained before hydriding. Patterns (B) and (C) are obtained after 10 cycles and 10K cycles, respectively, in dehydrided condition. Pattern (D) is obtained after 10K cycles in hydrided condition.

The XRPD patterns obtained from the 10 000 cycled hydride, $La_{0.9}Gd_{0.1}Ni_5H_y$, did not show any analyzable hydride peaks. A high background pattern was observed in spite of repeated attempts to acquire the data at very slow scanning rates of 0.002° 2θ for 2 s on our Philips diffractometer. Nor did attempts to obtain the patterns using a Rigaku rotating anode diffractometer (pattern D in Fig. 8) yield the major (111) and (200) reflections expected from a crystalline hydride phase, suggesting formation of microcrystalline or amorphous phases. A possible problem of absorption of X-rays by the capillary was ruled out because the Bragg peak of the Si standard is observed in pattern D in Fig. 8.

Line profile analyses revealed microstrain and particle-size effects in both 10 and 10 000 cycled dehydrided $La_{0.9}Gd_{0.1}Ni_5$. The XRPD patterns

clearly show ($hh0$), ($h0h$), (001) peak broadening. By applying the Warren–Averbach method $\langle \epsilon^2 \rangle^{1/2}$ strains were calculated from the X-ray data and are shown in Fig. 9 in [001] and [−110] as a function of column length, L. The size coefficients are plotted as a function of L in Fig. 10.

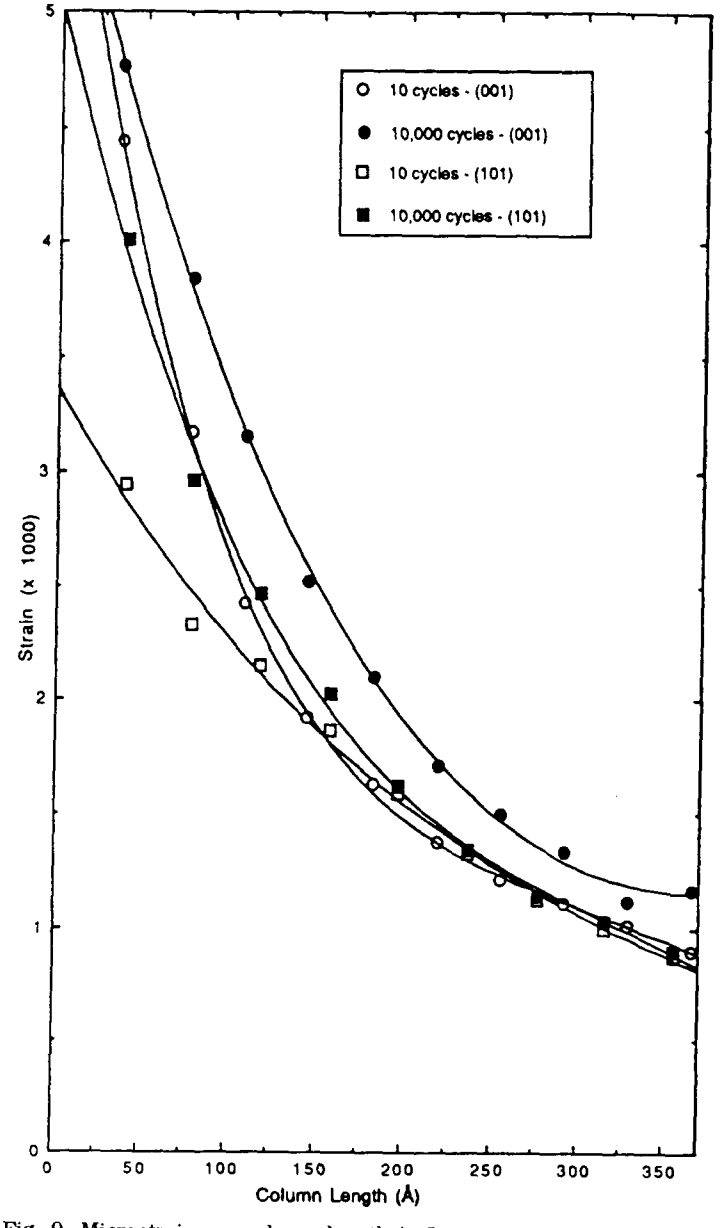

Fig. 9. Microstrain *vs.* column length in $La_{0.9}Gd_{0.1}Ni_5$ in (001) and (101) planes.

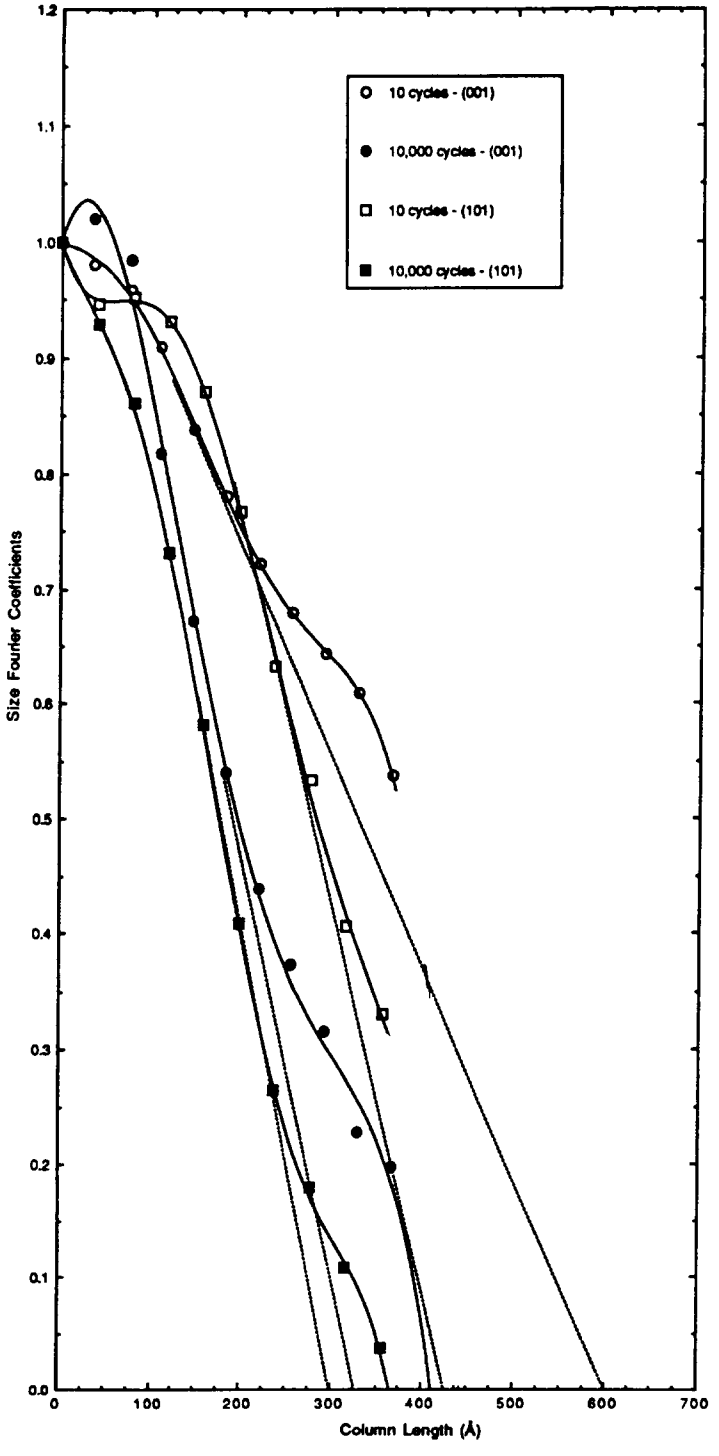

Fig. 10. Particle-size determination for $La_{0.9}Gd_{0.1}Ni_5$ in (001) and (101) planes after 10 and 10 000 cycles using Fourier size coefficients.

3.2. The system $LaNi_{4.8}Sn_{0.2}$ hydrogen

The static pressure–composition isotherm taken at 25, 42 and 93 °C show absorption/desorption plateau pressure ratios of 52/48, 105/110 and 660/610 (in KPa) respectively (Fig. 11). These plateaus give no indications of phase separation and the hydriding pressures and hysteresis are significantly lower than those of $La_{0.9}Gd_{0.1}Ni_5$ at all temperatures. The van't Hoff plots from the mid-plateau pressures clearly illustrate this in Fig. 4. After 10, 1500 and 10 000 thermal cycles static pressure–composition isotherms obtained for $LaNi_{4.8}Sn_{0.2}$ are shown in Fig. 12. The hydrogen capacities of $LaNi_{4.8}Sn_{0.2}$ are less than that of pure $LaNi_5$, but the decrease in reversible hydrogen capacity is minimal after 1500 absorption/desorption thermal cycles. There is just a 10% loss of hydrogen capacity between the 10 and 1500 cycles and less than 15% loss after 10 000 cycles. The thermally aged $LaNi_{4.27}Sn_{0.24}$ yielded nearly the same plateau pressure as that of thermally cycled $LaNi_{4.8}Sn_{0.2}$ samples and with a little loss of hydrogen capacity. The pressure–composition isotherms for $LaNi_{4.27}Sn_{0.24}$ obtained at 25 °C (298 K) before and after thermal aging are shown in Fig. 13.

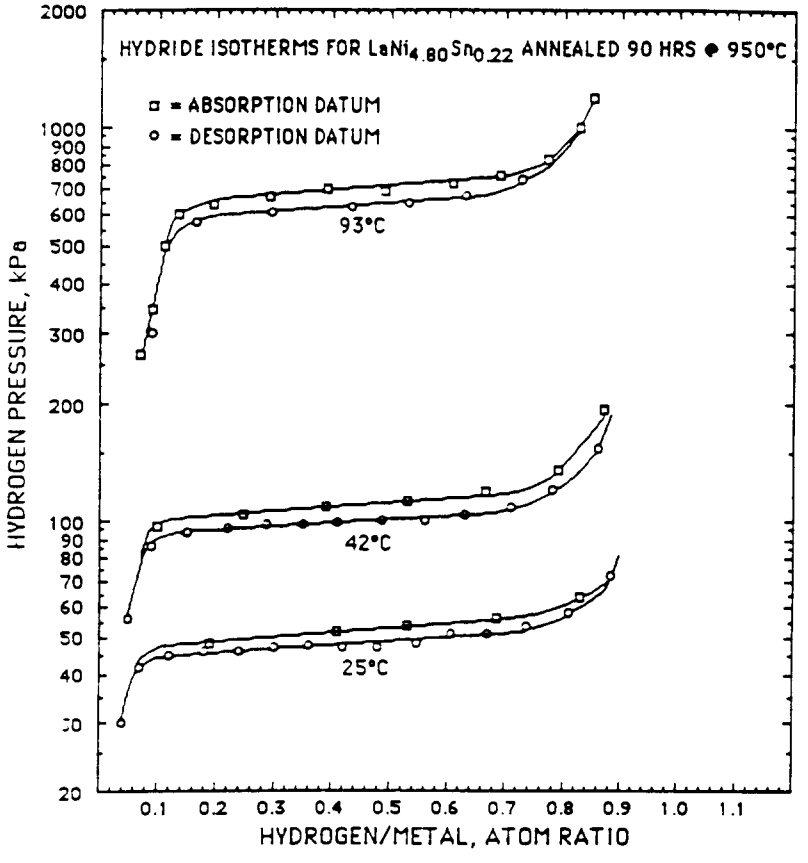

Fig. 11. Hydrogen pressure *vs.* hydrogen content in $LaNi_{4.8}Sn_{0.22}$ at 25, 42 and 93 °C.

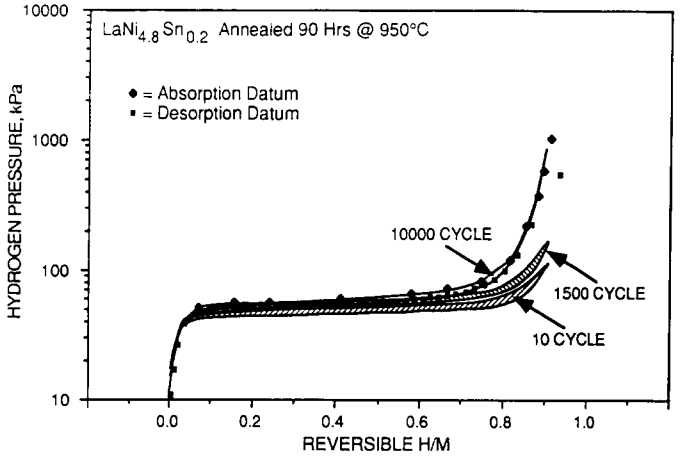

Fig. 12. Hydrogen pressure *vs.* hydrogen content in $LaNi_{4.8}Sn_{0.22}$. Compound retained almost all hydrogen capacity even after 10 000 cycles.

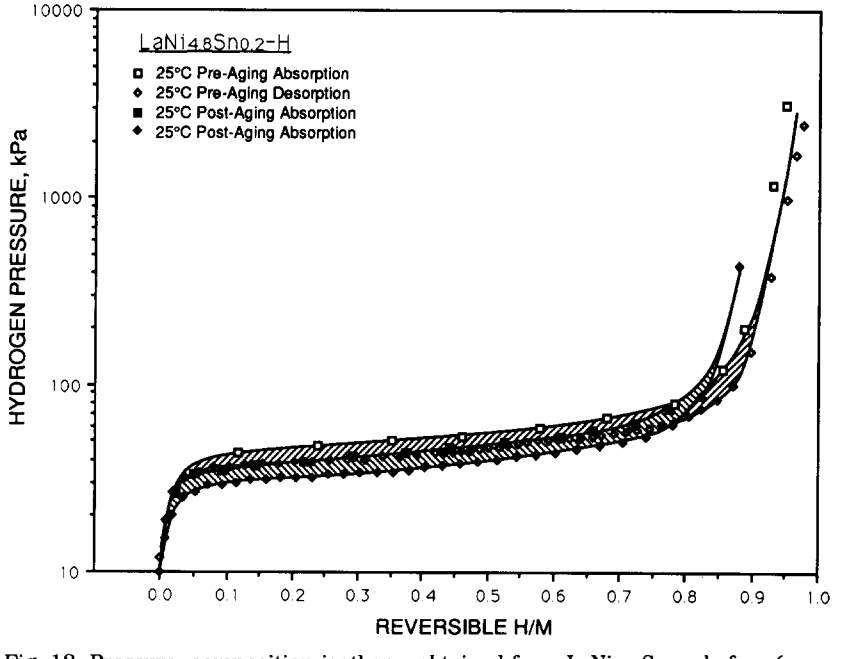

Fig. 13. Pressure–composition isotherm obtained from $LaNi_{4.27}Sn_{0.24}$ before (open data points) and after thermal aging at 25 °C.

The XRPD patterns of the $LaNi_{4.8}Sn_{0.2}$ alloy before and after 10 000 thermal cycles are shown in Fig. 14A and 14B respectively. There are no significant changes in the broadening of Bragg peaks after 10 000 hydriding cycles, in dehydrided condition, as seen in pattern B. The hydrides of $LaNi_{4.8}Sn_{0.2}$ remain in well crystallized condition after 10 000 and 10 cycles, as shown by the sharp Bragg peaks in Fig. 14C and 14D respectively. The

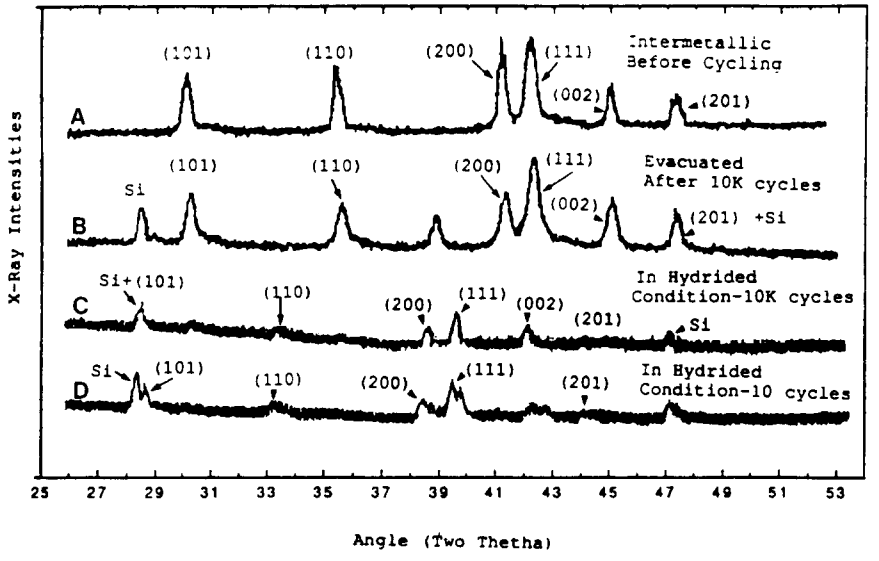

Fig. 14. X-ray diffraction patterns for $LaNi_{4.8}Sn_{0.22}$. This was the only compound to retain hexagonal structure in hydrided condition, even after 10 000 cycles.

pattern for the 10-cycled hydride shows well separated $Si_{(111)}$ internal standard and $LaNi_{4.8}Sn_{0.2}H_{y(101)}$ peaks. However, in the case of 10 000 cycled hydrides the two peaks overlap, indicating an increase in the c dimension after 10 000 cycles. It can be noted that there are α-phase Bragg peaks, of low intensity, in the hydride patterns (Fig. 14C and 14D). This suggests that the hydride phase is not fully saturated with hydrogen and that losses may have occurred during the loading of hydride powders in the capillaries.

The line broadening in thermally cycled, dehydrided $LaNi_{4.8}Sn_{0.2}$, or thermally aged $LaNi_{4.27}Sn_{0.24}$ is significantly smaller than that of $La_{0.9}Gd_{0.1}Ni_5$. The microstrain and particle sizes obtained by the Cauchy multiple-line method for both $LaNi_{4.8}Sn_{0.2}$ and $La_{0.9}Gd_{0.1}Ni_5$ are shown in Fig. 15. The D and e values are obtained from the least square straight-line fit to the data. The broadening in 10-cycle $LaNi_{4.8}Sn_{0.2}$ peaks is mainly due to particle-size effects using the (001), (002), (101) and (202) peaks, and strains are very low, as indicated by the slope of the line in Fig. 15. There is a slight increase in the strain value after 10 000 cycles, with few changes in particle size.

4. Discussion

The loss of hydrogen capacity and changes in pressures due to substitution (without any thermal cycling or aging) are well established [21]. In our case the pressure–composition isotherms show vastly different hydriding pressures for $LaNi_{4.8}Sn_{0.2}H_y$ with a saturated stoichiometry of $y = 5.8$ and $La_{0.9}Gd_{0.1}Ni_5H_y$ with $y = 6$ at room temperature, whereas for pure $LaNi_5H_y$, $y = 6.7$ [15]. The standard thermodynamic parameters $\Delta H°$, $\Delta S°$ and $\Delta G°$ are calculated from

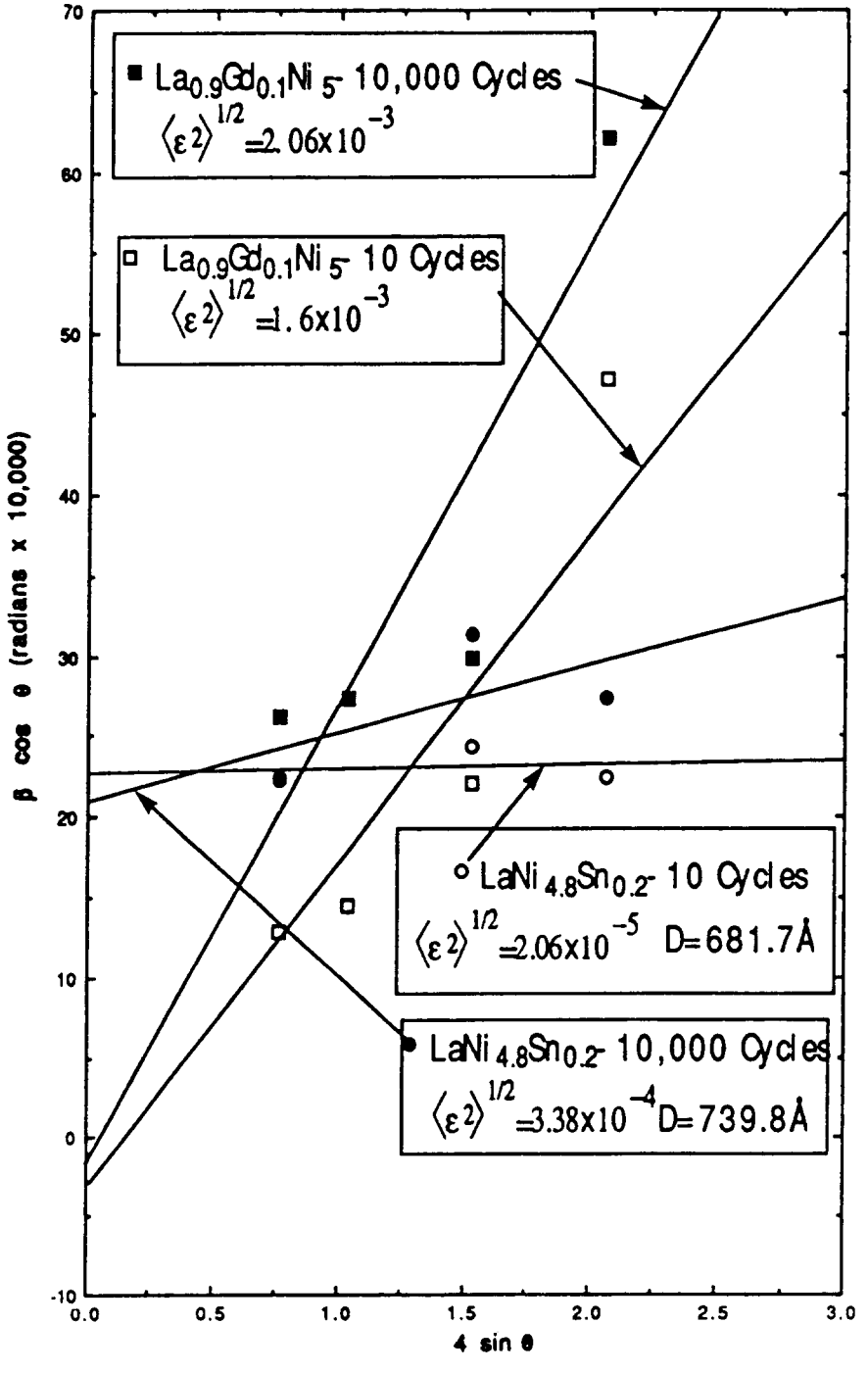

Fig. 15. Microstrain and domain sizes obtained by Cauchy method for $La_{0.9}Gd_{0.1}Ni_5$ and $LaNi_{4.8}Sn_{0.22}$.

the van't Hoff plots in Fig. 4. The properties of $\beta \rightarrow \alpha$ transformations, representing absorption and desorption reactions, at 298.15 K are tabulated in Table 1. The $\Delta G°$ at 198.15 K for the endothermic $\beta \rightarrow \alpha$ desorption of $LaNi_{4.8}Sn_{0.2}H_y$, $La_{0.9}Gd_{0.1}Ni_5H_y$ and $LaNi_5H_y$ are +1.8 and −2.9 and −1.49 kJ (mol H_2)$^{-1}$ respectively.

The hysteresis in $La_{0.9}Gd_{0.1}Ni_5H_y$ is greater than that of $LaNi_{4.8}Sn_{0.2}H_y$ at all the temperatures for which data have been acquired. The absorption/desorption plateau pressure ratios (P_A/P_D) for these two compounds, together with the differences in free energy, $(\Delta G°_A - \Delta G°_D)/RT$, are listed in Table 2. These pressure ratios in as-activated samples (after 10 cycles) in Table 2 for $LaNi_{4.8}Sn_{0.2}$ are comparable with those of Mendelsohn *et al.* [2], who report a value of $P_A/P_D = 1.038$ for $La_{1.05}Ni_{4.6}Sn_{0.4}$ with a $P_D = 0.156$ atm at 32 °C. Oliver *et al.* [22] have reported desorption pressures of $P_D = 0.25$

TABLE 1

The free energies for absorption (A) and desorption (D) reactions at 298.15 K for $La_{0.9}Gd_{0.1}Ni_5$ and $LaNi_{4.8}Sn_{0.2}$

	Reaction/Transformations	$\Delta G°$ (kJ(mol H_2)$^{-1}$)
		$\Delta H - \Delta S \cdot T$
A	1/3 $LaNi_{4.8}Sn_{0.2} + H_2 \rightarrow$ 1/3 $LaNi_{4.8}Sn_{0.2}H_y$	−34 500 + 110.0 T
D	1/3 $LaNi_{4.8}Sn_{0.2}H_y \rightarrow$ 1/3 $LaNi_{4.8}Sn_{0.2} + H_2$	34 500 − 109.7 T
A	1/3 $La_{0.9}Gd_{0.1}Ni_5 + H_2 \rightarrow$ 1/3 $La_{0.9}Gd_{0.1}Ni_5H_y$	−29 200 + 107.7 T
D	1/3 $La_{0.9}Gd_{0.1}Ni_5H_y \rightarrow$ 1/3 $La_{0.9}Gd_{0.1}Ni_5 + H_2$	29 200 − 107.7 T
A	1/3 $LaNi_5H_y \rightarrow$ 1/3 $LaNi_5 + H_2$ [15]	30 900 − 108.62 T

TABLE 2

The absorption/desorption pressure ratios $\ln(P_A/P_D)$ for $La_{0.9}Gd_{0.1}Ni_5$, $LaNi_{4.8}Sn_{0.2}$ and $LaNi_5$ as a function of temperature

Temperature		$LaNi_{4.8}Sn_{0.2}$		$La_{0.9}Gd_{0.1}Ni_5$		$LaNi_5$
K	°C	$\ln(P_A/P_D)$	$(\Delta G°_A - \Delta G°_D)/RT$	$\ln(P_A/P_D)$	$(\Delta G°_A - \Delta G°_D)/RT$	$\ln(P_A/P_D)$[a]
277	4	–	−3.614	0.223	0.722	–
298	25	0.08	−1.448	0.154	2.56	0.14
315	42	0.049	0.08	0.194[b]	3.848	–
318	45	0.087[b]	0.334	0.214[b]	4.063	0.14
328	55	0.057[b]	1.147	0.201[b]	4.752	0.13
338	65	0.036[b]	1.913	–	5.399	0.12
348	75	0.026[b]	2.634	0.192	6.010	–
366	93	0.125	3.833	–	7.024	–

[a]From ref. 23.

[b]Estimated from van't Hoff plot.

atm at 25 °C for $LaNi_{4.7}Sn_{0.3}$. The pressure ratios P_A/P_D for $LaNi_{4.8}Sn_{0.2}$ are $(1.083)_{10\ cyc}$, $(1.3)_{10\,000\ cyc}$ and $(1.4)_{TA}$. The pressure ratios for $LaNi_5$ are included in Table 2 for comparison.

There is no definitive correlation between the pressure ratio and the degradation of the hydrides, but it appears that the lower the hysteresis the less the degradation. For example, the $LaNi_{4.8}Sn_{0.2}$ hydride has both very low hysteresis and little degradation, in contrast to the behavior found for the hydrides of $La_{0.9}Gd_{0.1}Ni_5$ and $LaNi_5$, as indicated in Table 2 and Figs. 3 and 6. The absorption/desorption pressure ratios are independent of the temperature and the enthalpy remains constant between 4 and 93 °C. Because the entropy increases with temperature, the $(\Delta G°_A - \Delta G°_D)/RT$ values in Table 2 are larger at higher temperatures. Birnbaum *et al.* [24] have suggested that thermal hysteresis reflects the total amount of plastic work done during the hydriding and the dehydriding cycles. The pressure plateaus suggest that P_A or P_D are both non-equilibrium since the dislocations may be generated during absorption and desorption cycles. Lundin and Lynch [23], on the basis of the atomistic model, have suggested that more negative energy of hydride formation lowers the hydriding plateau pressures. Thus lower accumulation of strain is expected during $\alpha \rightarrow \beta$ transformation, if the hysteresis is small. The nearly constant ln P_A/P_D shown in Table 2 is in agreement with the model of Lundin and Lynch [23].

On the basis of X-ray and isotherm data obtained it is indicative that if the hydrides remain well crystallized after 10 000 cycles there is very little loss in hydrogen capacity. The X-ray patterns in Fig. 8 show that after 10 000 cycles $La_{0.9}Gd_{0.1}Ni_5$ hydride is either amorphous or microcrystalline, but that the latter may be more likely. If a mosaic structure of $La_{0.9}Gd_{0.1}Ni_5$ develops in which individual grains have many very small independently diffracting domains coupled with strain in the lattice, due to introduction of hydrogen, then the diffraction peaks broaden significantly to the extent that they are not observable in the patterns [25]. However, the $LaNi_{4.8}Sn_{0.2}$ hydride retains excellent crystallinity even after 10 000 cycles, as shown in Fig. 14. In the activated samples of $LaNi_{4.8}Sn_{0.2}$ hydride, the volume increase is approximately 18.7%, with only a small additional increase of 0.2% after 10 000 cycles. The splitting of peaks in 10 cycle $LaNi_{4.8}Sn_{0.2}H_y$ may be due to formation of an additional γ-hydride phase, as suggested by Matsumoto and Matsushita [12]. However, the pressure of difference may in our case be so small that it is not observed in the pressure-composition plots in Figs. 11 and 12. Attempts made to dehydride this 10 cycle $LaNi_{4.8}Sn_{0.2}H_y$ (Table 3: 2b) sample by evacuation were not successful and a metastable hydride phase formed whose lattice parameters are 5.3733 Å (±0.0034) and 4.2202 Å (±0.00215). The metastable hydride parameters are lower than those observed for 10-cycled $LaNi_{4.8}Sn_{0.2}H_y$ in evacuated condition but do not match with those reported for γ-$LaNi_5H_y$ [12].

In the case of $La_{0.9}Gd_{0.1}Ni_5$, the XRPD patterns show that the precipitation of Ni metal has occurred after 10 000 cycles; therefore, disproportionation may have occurred as proposed by Cohen *et al.* [7] and Gamo *et al.* [4].

TABLE 3

Lattice parameters of hexagonal $LaNi_{4.8}Sn_{0.22}$ and $La_{0.9}Gd_{0.1}Ni_5$. Intermetallics and hydrides cycled 10 and 10 000 times in this study. Also shown are the lattice parameters for the thermally aged (TA) sample. Values in parentheses represent standard deviations in lattice parameters.

Materials		Lattice parameters				
		Cycles	a_0 (Å)	c_0 (Å)	c/a	Cell volume (Å^3)
1a	$La_{0.9}Gd_{0.1}Ni_5$	0	5.0538 (0.0012)	4.0268 (0.0006)	0.797	89.069
1b	$La_{0.9}Gd_{0.1}Ni_5H_y$[a]	10	–	–	–	–
1c	$La_{0.9}Gd_{0.1}Ni_5$[c]	10	5.0039 (0.0025)	3.9866 (0.0097)	0.797	86.4471
1d	$La_{0.9}Gd_{0.1}Ni_5$[b,d]	10 000	4.9879 (0.0097)	3.9950 (0.0055)	0.801	86.0761
1e	$La_{0.9}Gd_{0.1}Ni_5$(TA)[b]	–	5.0354 (0.0051)	4.0677 (0.0059)	0.808	89.317
2a	$LaNi_{4.8}Sn_{0.2}$	0	5.0723 (0.0038)	4.0389 (0.0025)	0.796	89.992
2b	$LaNi_{4.8}Sn_{0.2}H_y$	10	5.3785 (0.0065)	4.2642 (0.0036)	0.793	106.829
2c	$LaNi_{4.8}Sn_{0.2}H_y$	10 000	5.3850 (0.0012)	4.2683 (0.0006)	0.793	107.188
2d	$LaNi_{4.8}Sn_{0.2}$[d]	10 000	5.0751 (0.0225)	4.0280 (0.0125)	0.794	89.848
2e	$LaNi_{4.8}Sn_{0.2}$(TA)	–	5.0453 (0.0017)	4.0082 (0.0018)	0.794	88.357
3a	$LaNi_5$ (ref. 28)	–	5.017	3.982	0.793	86.800
3b	$LaNi_5$ (ref. 3)	–	5.017	3.987	0.795	86.909

[a]Lattice parameters could not be obtained because the major Bragg peaks were not observed.
[b]Additional peaks of metallic nickel phase.
[c]Evacuated after 10 hydriding cycles.
[d]Evacuated after 10 000 hydriding cycles.

However, the peaks for a LaH_2 phase are not observed in the XRPD patterns. The Ni peaks are broadened, suggesting formation of small grains or clusters of nickel which may be under compression in the hexagonal matrix. It is estimated that the particle size of this Ni phase is approximately 150 Å. It should be noted that this Ni phase is not present in the alloy either before or after 10 hydriding cycles. The fact that the nickel phase precipitates after prolonged cycling is consistent with the formation of La-rich compounds. Han and Lee [26] have suggested formation of amorphous $LaNi_3$ and La_2Ni_7 hydrides during cycling. If after 10 000 cycles there is partial disproportionation and amorphous compounds are formed, $La_{0.9}Gd_{0.1}Ni_5$ hydrides may form small clusters of $La_{0.9}Gd_{0.1}Ni_3H_y$ and $La_{1.9}Gd_{0.1}Ni_7H_y$ or LaH_2 hydrides that are not detected in the X-ray diffraction patterns in Fig. 8, pattern D. Mordkovich *et al.* [11] performed thermobaric cycling of $LaNi_5$ and reported

observing precipitation of Ni along with LaH or LaH_2. It is interesting to note the recovery of the hexagonal structure of $La_{0.9}Gd_{0.1}Ni_5$ after evacuating the 10 000 cycled microcrystalline or amorphous hydride (Fig. 8, pattern C). Our desorption studies, after thermal aging of $La_{0.9}Gd_{0.1}Ni_5$ at 453 K for 256 h, show that the pressures generated by heating $La_{0.9}Gd_{0.1}Ni_5$ in the range 200–400 K are between 500 and 1100 kPa. These pressures are several orders of magnitude larger than equilibrium pressures observed for LaH_2 by Korst and Warf [27] and do not support the formation of LaH_2 as the primary decomposition products.

In general, there are decreases in volumes of the unit cells after 10 000 thermal cycles for both the compounds under consideration, as shown in Table 3. These results suggest that in addition to the microstrains in the crystal lattice there are long-range strains indicated by the shifts in peaks. These shifts are more pronounced for the $La_{0.9}Gd_{0.1}Ni_5$ in Fig. 8 as compared with that of $LaNi_{4.8}Sn_{0.2}$ in Fig. 14, but Ni precipitation during the cycling may cause disorder in the lattice, as indicated by the changes in the intensities of the peaks. Thus it is difficult to ascertain realistic long-range strain values. The volume changes, $(\Delta V/V)_{0\rightarrow 10\,K}$, are greater in the case of highly strained $La_{0.9}Gd_{0.1}Ni_5$ (-3.4×10^{-2}) as compared with that of $LaNi_{4.8}Sn_{0.2}$ (-1.6×10^{-3}); however the c/a ratios are not significantly different. The lattice parameters of $LaNi_5$ from [3, 28] are also listed in Table 3.

The microstrains and domain size effects in dehydrided $La_{0.9}Gd_{0.1}Ni_5$ show in Fig. 9 and 10 are discussed in this paragraph. It is apparent that there is significant broadening of the Bragg peaks of dehydrided $La_{0.9}Gd_{0.1}Ni_5$ (Fig. 8). From Table 4 the average domain size for the 10 cycle $La_{0.9}Gd_{0.1}Ni_5$ is 513 Å with an anisotropy of $\{D_{\text{eff }[001]}/D_{\text{eff }[101]}\}_{10\text{cyc}}=1.42$. This average domain size decreases to 313 Å with $\{D_{\text{eff }[001]}/D_{\text{eff }[101]}\}_{10\,000\text{cyc}}=1.08$, after 10 000 cycles. We have conventionally reported the strains at $D_{\text{eff}}/2$ for [101] and [001] directions in Table 4, but for comparison of the microstrains for 10 and 10 000 cycled samples, a fixed distance of 100 Å is used. The r.m.s. strains are almost isotropic after the initial 10 cycles and the $\{\langle\epsilon^2\rangle^{1/2}_{[101]}/\langle\epsilon^2\rangle^{1/2}_{[001]}\}_{10\text{cyc}}=\{2.5\times10^{-3}/2.4\times10^{-3}\}=1.04$. After 10 000 cycles some anisotropy has developed and the strain ratio is $\{\langle\epsilon^2\rangle^{1/2}_{[101]}/\langle\epsilon^2\rangle^{1/2}_{[001]}\}_{10\,000\text{cyc}}=\{3.4\times10^{-3}/2.9\times10^{-3}\}=1.17$, at a distance of $(L)=100$ Å (Fig. 9). As can be noted from Table 4 and Fig. 15, the average microstrain values obtained by the Cauchy method agree closely with those computed by the Warren–Averbach method at $D_{\text{eff}}/2$. However, we could not obtain the domain sizes for $La_{0.9}Gd_{0.1}Ni_5$ by this Cauchy method. A significant amount of strain is accumulated in the lattice during the first 10 cycles but after prolonged cycles the strains do not increase proportionately. This may be attributed to the recovery processes and fracture of the particles relieving the strain during each thermal cycle. The domain sizes decrease after prolonged cycling. The trends in changes of the D_{eff} and strain are similar to those obtained for $LaNi_5$ by Josephy *et al.* [10] (Table 4). The strains for $LaNi_5$ are highly anisotropic as compared with that of $La_{0.9}Gd_{0.1}Ni_5$. Similar results have been obtained by Nomura *et al.* [13] but the domain size reported for

TABLE 4

The microstrain distribution and particle size in $La_{0.9}Gd_{0.1}Ni_5$ and $LaNi_{4.8}Sn_{0.2}$ determined by the Warren–Averbach and the Cauchy methods, respectively, after 10 and 10 000 thermal cycles and after thermal aging (TA). Microstrains and particle sizes for $LaNi_5$ from Josephy *et al.* [10] are included for comparison

	D_{eff}	$\langle\epsilon^2\rangle^{1/2}\times10^3$	D_{eff}	$\langle\epsilon^2\rangle^{1/2}\times10^3$	D_{av}	$\langle\epsilon^2\rangle^{1/2}\times10^{3a}$	
	[101]		[001]		Average		
$La_{0.9}Gd_{0.1}Ni_5$ (this study)							
10 cycles	425 Å[b]	1.1[b]	600 Å[b]	1.4[b]	513 Å[b]	1.3[b]	1.6[b]
10 000 cycles	300 Å[b]	2.6[b]	325 Å[b]	2.0[b]	313 Å[b]	2.3[b]	2.06[b]
TA	–	–	270 Å[b]	2.4[b]	–	–	
$LaNi_{4.8}Sn_{0.2}$ (this study[b])							
10 cycles	–	–	–	–	681 Å[a]	–	0.0206[a]
10 000 cycles	–	–	–	–	740 Å[a]	–	0.338[a]
$LaNi_5$ (estimated from Josephy *et al.* [10])							
10 cycles	820 Å	3.7	820 Å	0.4	820	2.1	–
10 000 cycles	525 Å	7.4	626 Å	1.2	576	4.3	–

[a]Determined by Cauchy function.
[b]Determined by Warren–Averbach method.

$LaNi_5$ of $D = 133$ Å after initial activation is smaller than that of $La_{0.9}Gd_{0.1}Ni_5$ and $LaNi_5$ in ref. 10.

The domain sizes and microstrain estimated from Fig. 15 and summarized in Table 4 clearly indicate that the microstrain in $LaNi_{4.8}Sn_{0.2}$ is two orders of magnitude smaller than that of $La_{0.9}Gd_{0.1}Ni_5$ after 10 cycles. It appears that the domain sizes and microstrain increase after 10 000 cycles, but because these values are averaged for (001), (002), (101) and (202) reflections the errors in estimation are high. A possible explanation for this low microstrain in $LaNi_{4.8}Sn_{0.2}$ is that there are strong interactions of Sn with Ni which may stabilize the Ni sublattice in the 2*c* layers with stable Ni_3Sn bounded cages. We base this on Percheron-Guegan and Lartigue's [29], two-dimensional long-range diffusion, model of hydrogen in which the "bounded" cages may provide an easy path for hydrogen diffusion.

The isotherms in Fig. 12 for $LaNi_{4.8}Sn_{0.2}$ taken after 10 000 cycles at 298 K showed low hysteresis and a reversible hydrogen capacity over 90% of the value, after 10 cycles. Park and Lee [9] reported that a similar substituted alloy, $LaNi_{4.7}Al_{0.3}$, had its capacity reduced to about 86% after 2500 cycles between 303 K and 458 K. Chandra and Lynch [30] reported a 5.6% loss for $LaNi_{4.75}In_{0.27}$ during the first 1500 cycles between room temperature and 398 K; however, an almost 80% of capacity is observed after 2483 cycles. Thus, it appears that $LaNi_{4.8}Sn_{0.2}$ is more stable than either $LaNi_{4.7}Al_{0.3}$ or $LaNi_{4.75}In_{0.27}$ during thermal cycling. It would be interesting to conduct experiments on thermal degradation using the other group IVA elements, such as Si and Ge substituted $LaNi_{5-y}M_y$.

5. Conclusions

The hydrogen capacity of $LaNi_{4.8}Sn_{0.2}$ remains virtually unaffected after 10 000 thermal cycles with very low hysteresis during the absorption/desorption cycle, and the hydrides remain crystalline after 10 000 cycles. Minimum degradation of the hydriding properties is observed in the thermally aged $LaNi_{4.75}Sn_{0.24}$ hydride. In contrast, the hydrogen capacity for $La_{0.9}Gd_{0.1}Ni_5$ is reduced significantly after 10 000 cycles and after thermal aging. After 10 000 cycles, the hydride phase remains well crystallized in the case of $LaNi_{4.8}Sn_{0.2}$, whereas for the $La_{0.9}Gd_{0.1}Ni_5$ it appears to be amorphous or microcrystalline, with nickel-phase precipitation. After prolonged cycling, the microstrains after desorption of hydrogen are large and the domain sizes small for the $La_{0.9}Gd_{0.1}Ni_5$ and vice versa for $LaNi_{4.8}Sn_{0.2}$. The thermally aged samples of $La_{0.9}Gd_{0.1}Ni_5$ show similar degradation to that observed by Sandrock *et al.* [17] for $LaNi_5$, but the slope of the isotherm is steeper as compared with $LaNi_5$. The thermally aged samples of $La_{0.9}Gd_{0.1}Ni_5$ do not show any hysteresis but the thermally cycled samples show hysteresis. The mechanism for degradation of the structure and the generation of a steep slope in the absorption/desorption plateau in the $La_{0.9}Gd_{0.1}Ni_5$ is not clear at this time. However, it seems very likely that cycling promotes the formation and stabilization of the intermediate γ-$LaNi_5H_{x=3-4}$ [11–13, 31, 32] at the expense of β-$La_{0.9}Gd_{0.1}Ni_5H_x$ but with additional propensity toward microcrystalline-phase segregation.

6. Acknowledgments

The authors wish to acknowledge the NASA (Lyndon B. Johnson Space Center) for the support of this research under NASA Contract No. NAS 9-17549 and also the generous support of Hydrogen Consultants Inc. (HCI). We thank Keith Stever and Kay Blakely of the US Bureau of Mines, Reno, for the use of X-ray instrumentation for some of this research, Dr. Sampath Iyengar of B. P. America, Ohio for the use of the Rigaku diffractometer and Renee A. Lynch, University of Nevada, for her help with the lattice parameter computations. The paper is based in part on a Master's thesis submitted by S. W. L.

References

1 M. Nagel, Y. Kornazaki and Y. S. Suda, *J. Less-Common Met., 120* (1986) 45.
2 M. Mendelsohn, M. Greun and A. Dwight, *Inorg. Chem., 18* (1979) 3343.
3 H. H. van Mal, K. H. J. Buschow and A. R. Miedema, *J. Less-Common Met., 35* (1974) 65.
4 T. Gamo, Y. Moriwaki, N. Yanagihara and T. Iwaki, *J. Less-Common Met., 89* (1983) 495.
5 R. L. Cohen, K. W. West and K. H. J. Buschow, *Solid State Commun., 25* (1978) 293.
6 R. L. Cohen, K. W. West and J. H. Wernick, *J. Less-Common Met., 70* (1980) 229.

7 M. J. Benham, D. K. Ross, C. Lartigue and A. Percheron-Guegan, *Z. Phys. Chem. N. F., New York, 147* (1987) 205.
8 K. H. J. Buschow and A. R. Meidema, *Proc. Int. Symp. for Energy Storage, Geilo, August 14–19, 1977*, Pergamon, Oxford, 1978, pp. 235–249.
9 J. M. Park and J. Y. Lee, *Mater. Res. Bull., 22* (1987) 455.
10 Y. Josephy, E. Bershadshky and M. Ron, *J. Less-Common Met., 172* (1991) 997.
11 V. Z. Mordkovich, N. N. Korstyshevsky, Yu. K. Baychitok, E. I. Mazus, N. V. Dudakova and V. P. Mordovin, *Int. J. Hydrogen Energy, 15* (1990) 723.
12 T. Matsumoto and A. Matsushita, *J. Less-Common Met., 123* (1986) 135.
13 K. Nomura, H. Uruno and S. Ono, H. Shinozuka and S. Suda, *J. Less-Common Met., 107* (1985) 221.
14 M. Doyama, S. Samiya and R. P. H. Chang (eds.), *Proc. MRS Int. Mtg. on Advanced Materials, May 31–June 3, 1988, Sunshine City, Ikebukuro, Tokyo, Japan, Hydrogen Absorbing Materials — Catalytic Materials*, Vol. 2, Materials Research Society, Pittsburgh, PA, 1989.
15 P. D. Goodel, *J. Less-Common Met., 99* (1984) 1.
16 G. H. Kim and Jai-Young Lee, *J. Less-Common Met., 132* (1987) 123.
17 G. D. Sandrock, *Z. Phys. Chem. N. F., 164* (1982) 225.
18 J. F. Lynch and J. J. Reilly, *J. Less-Common Met., 87* (1987) 123.
19 H. P. Klug and L. E. Alexander, *X-ray Diffraction Procedures*, Wiley, 1974, pp. 661–666.
20 B. E. Warren, *X-ray Diffraction*, Addison Wesley, Reading, MA, 1969.
21 A. Percheron-Guegan, C. Lartigue and J. C. Archard, *J. Less-Common Met., 109* (1985) 287.
22 F. W. Oliver, W. Morgan, E. C. Hammond, S. Wood and L. May, *J. Appl. Phys., 57* (1985) 3250.
23 C. E. Lundin and F. E. Lynch, *Proc. Int. Conf. on Alternate Energy Sources, Miami, FL*, University of Miami Press, 1979.
24 H. K. Birnbaum, *J. Less-Common Met., 104* (1984) 357; H. K. Birnbaum, M. L. Grossbeck and M. Amano, *J. Less-Common Met., 49* (1976) 357.
25 L. H. Schwartz and J. B. Cohen, *Diffraction From Materials*, Academic Press, New York, 1977.
26 J. I. Han and J.-Y. Lee, *Int. J. Hydrogen Energy, 13* (1988) 577.
27 W. L. Korst and J. C. Warf, *Inorg. Chem., 5* (1966) 1719.
28 K. H. J. Buschow and H. H. van Mal, *J. Less-Common Met., 29* (1972) 203.
29 A. Percheron-Guegan and C. Lartigue, *Mater. Sci., Forum., 31* (1988) 125.
30 D. Chandra and F. Lynch, *Rare Earths*, The Metallurgical Society, Warrendale, PA, 1988, p. 83.
31 A. L. Shilov, M. E. Kost and N. T. Kunzetsov, *J. Less-Common Met., 144* (1988) 23.
32 P. Selvam and K. Yvon, *J. Less-Common Met., 171* (1991) L17.